Micro Structure and Corrosion Resistance of Zn Composites Films Produced by Pulse Electrolysis from a Insoluble Particle-free Solution Containing Zr Ions

Sota, Toyokuni
Graduate School of Engineering, Kyushu, University

Oue, Satoshi
Faculty of Engineering, Kyushu University

Taninouchi, Yu-ki
Faculty of Engineering, Kyushu University

Nakano, Hiroaki
Faculty of Engineering, Kyushu University

出版情報：ISIJ International. 63 (11), pp.1908-1918, 2023-11-15. 日本鉄鋼協会
バージョン：

ISIJ International, Vol. 63 (2023), No. 11, pp. 1908–1918
https://doi.org/10.2355/isijinternational.ISIJINT-2023-270

Micro Structure and Corrosion Resistance of Zn Composites Films Produced by Pulse Electrolysis from a Insoluble Particle-free Solution Containing Zr Ions

Sota TOYOKUNI,[1)] Satoshi OUE,[2)] Yu-ki TANINOUCHI[2)] and Hiroaki NAKANO[2)]*

1) Graduate School of Engineering, Kyushu University, 744, Motooka, Nishi-ku, Fukuoka-shi, 819-0395 Japan.
2) Faculty of Engineering, Kyushu University, 744, Motooka, Nishi-ku, Fukuoka-shi, 819-0395 Japan.

(*Received on June 28, 2023; accepted on August 2, 2023; originally published in Tetsu-to-Hagané, Vol. 109, 2023, No. 8, pp. 684–694*)

The electrodeposition of an Zn–Zr compound composite is performed under pulsed and double-pulsed current conditions at 313 K in unagitated pH 2 sulfate solutions containing Zn^{2+} and ZrO^{2+} ions and polyethylene glycol. Under constant-current electrolysis at 5 000 $A{\cdot}m^{-2}$, coarse granular partial deposits containing Zr compounds are observed. Under pulse electrolysis, such coarse deposits are observed rarely; however, both deposited films containing Zr compounds and exfoliated films are observed. On the contrary, in double-pulse electrolysis at high (5 000 $A{\cdot}m^{-2}$) and low (500 $A{\cdot}m^{-2}$) current densities, coarse deposits are not observed while fine-particle deposits containing Zr compounds are observed. In double-pulse electrolysis at low current densities, the rate of hydrogen evolution decreases and Zn is deposited without the codeposition of Zr compounds; therefore, the continuous hydrogen evolution is suspended in some areas. That is, the area of hydrogen evolution appears to be random. Although Zr compounds are usually concentrated at the upper regions of the deposited films, regardless of the electrolysis method, it is found to have been codeposited even in the inner regions under double-pulse electrolysis. The corrosion current density in 3 mass% NaCl solution is the smallest for the films produced by double-pulse electrolysis, when comparing with the films obtained by pulse electrolysis and constant-current electrolysis. This can be attributed to the suppression of the reduction reaction of dissolved oxygen.

KEY WORDS: electrodeposition; zinc; zirconium compound; pulse electrolysis; double-pulse electrolysis; corrosion potential; corrosion current density; polyethylene glycol; composite films; hydrolysis.

1. Introduction

Composite electrodeposition, which codeposits fine particles such as oxides and organic compounds with metal matrixes, has been researched thoroughly, because it can endow materials with attractive properties such as corrosion resistance,[1–6)] wear resistance,[7–10)] and lubrication.[11–16)] In the conventional composite electrodeposition, particles are codeposited with a metal matrix from a suspension containing insoluble solid fine particles. However, because the fine particles gather easily in an electrolytic solution, it is difficult to uniformly disperse the codeposited fine particles in the deposited films, which can cause several problems during electrolysis, such as the clogging of pipes because of the sedimentation of agglomerated particles.[17)]

In Zn deposition from an acidic solution, the reduction of H^+ ions ($2H^+ + 2e^- \rightarrow H_2$) occurs as a side reaction, and the pH of the cathode layer increases.[18,19)] Therefore, when metal ions (M^{n+}) that hydrolyze at low pHs are added to electrolyte solutions as a second element, they turn into solid hydroxides or oxides via a hydrolysis reaction ($M^{n+} + nH_2O \rightarrow M(OH)_n + nH^+$) and codeposit with the deposited Zn films.[20–30)] Thus, the hydrolysis reaction during electrodeposition facilitates composite electrodeposition, without the need for the addition of insoluble solid particles into the electrolyte.

Previously, researchers added ZrO^{2+} ions that hydrolyzed at pHs lower than that of Zn^{2+} ions into the Zn electrolyte, and tried to codeposit the hydrolyzed products of ZrO^{2+} ions in the Zn films by electrolysis at a constant current density. However, Zn films with Zr hydroxide or oxide dispersed uniformly on the surface were not obtained.[25–30)] This was attributed to the hydrolysis reaction of ZrO^{2+} ions ($ZrO^{2+} + 3H_2O \rightarrow Zr(OH)_4 + 2H^+$ or $ZrO^{2+} + H_2O \rightarrow ZrO_2 + 2H^+$) proceeding partially on the Zn surface under electrolysis at a constant current density. If the hydrolysis

* Corresponding author: E-mail: nakano@zaiko.kyushu-u.ac.jp

reaction of ZrO^{2+} ions occurs at the site of the hydrogen evolution reaction, the hydrolysis reaction of ZrO^{2+} ions should proceed uniformly when the hydrogen evolution reaction occurs uniformly.

In pulse electrolysis, the current is turned on and off repeatedly. When the current is turned off, the hydrogen evolution is shut off immediately, which prevents the continuous evolution of hydrogen at the same site. In double-pulse electrolysis, the electrolysis is repeated at high and low current densities. The rate of hydrogen evolution decreases during electrolysis at low current densities, which weakens the hydrogen evolution reaction at that site.

The reduction of the dissolved oxygen in the corrosion reaction differs depending on the material of the substrate.[31] In the case of the deposited films obtained under constant-current electrolysis, when Zr hydroxide or oxide is codeposited with Zn, the reduction reaction of dissolved oxygen is suppressed on the deposited films.[29,30] The corrosion resistance of the Zn–Zr compound composite films appears to differ according to the codeposition state of the Zr compound.

Based on this background, in this study, Zn–Zr compound composite films are produced through pulse and double-pulse electrolysis from non-suspended solutions containing ZrO^{2+} ions, and their microstructure and corrosion resistance are investigated.

2. Experimental Section

The electrolyte composition and electrolysis conditions are presented in **Table 1**. The electrolytic solution was prepared by dissolving 0.052 mol·dm^{-3} reagent-grade $ZnSO_4{\cdot}7H_2O$ and 0.1 mol·dm^{-3} reagent-grade $Zr(SO_4)_2{\cdot}4H_2O$ in distilled and deionized water at room temperature. 1 g·dm^{-3} of polyethylene glycol (molecular weight of 6 000) was added as an additive. The pH of the solution was adjusted to 2 by adding small amounts of H_2SO_4 or NaOH aqueous solutions. In some experiments, deposited films of Zn, without Zr compounds, were produced using an Zn-only solution, by eliminating the 0.1 mol·dm^{-3} $Zr(SO_4)_2{\cdot}4H_2O$ from the solution mentioned above.

The films whose microstructure and corrosion resistance were to be evaluated were deposited through pulse electrolysis, wherein the current was turned on and off, and double-pulse electrolysis at high and low current densities; constant-current electrolysis was also performed for comparison. **Figure 1** shows the current waveforms under each electrolysis type. The current density (i_{on}) when the current turned on during pulse electrolysis was 5 000 A·m^{-2}, and the high (i_H) and low (i_L) current densities in double-pulse electrolysis were 5 000 and 500 A·m^{-2}, respectively. The current density (i_{const}) in constant-current electrolysis was 5 000 A·m^{-2}. For evaluating the current efficiency for Zn deposition and the Zr content in the deposited films, constant-current electrolysis was performed at 500 and 5 000 A·m^{-2}, respectively. The pulse period and duty ratio in both pulse and double-pulse electrolysis were 100 ms and 50%, respectively.

Prior to pulse and double-pulse electrolysis, a preliminary experiment was performed with constant-current electrolysis, and the Zr content in the deposited films (**Fig. 2**) and current efficiency for Zn deposition (**Fig. 3**) were measured. The Zr content in the deposited films was high at 5 000 A·m^{-2}; the current efficiency for Zn deposition was high and the Zr content in the films was low at 500 A·m^{-2}, indicating the suppression of hydrogen evolution at 500 A·m^{-2}. As observed from both the total polarization curve for Zn–Zr composite deposition and partial polarization curve for Zn deposition under constant-current electrolysis, the low current density (i_L) of 500 A·m^{-2} in double-pulse electrolysis lay in the region of Tafel's linear relationship in the partial polarization curve for Zn deposi-

Table 1. Electrolysis conditions.

Bath composition	$ZnSO_4{\cdot}7H_2O$	0.52 mol·dm^{-3}
	$Zr(SO_4)_2{\cdot}4H_2O$	0.1 mol·dm^{-3}
	pH	2
	Polyethylene glycol (M.W.6 000) 1 g·dm^{-3}	
Operating conditions	Current density	500, 5 000 A·m^{-2}
	Amount of charge	10^5 C·m^{-2}
	Temperature	313 K
	Cathode	Cu (2 cm×1 cm)
	Anode	Pt (2 cm×1 cm)
	Quiescent bath	

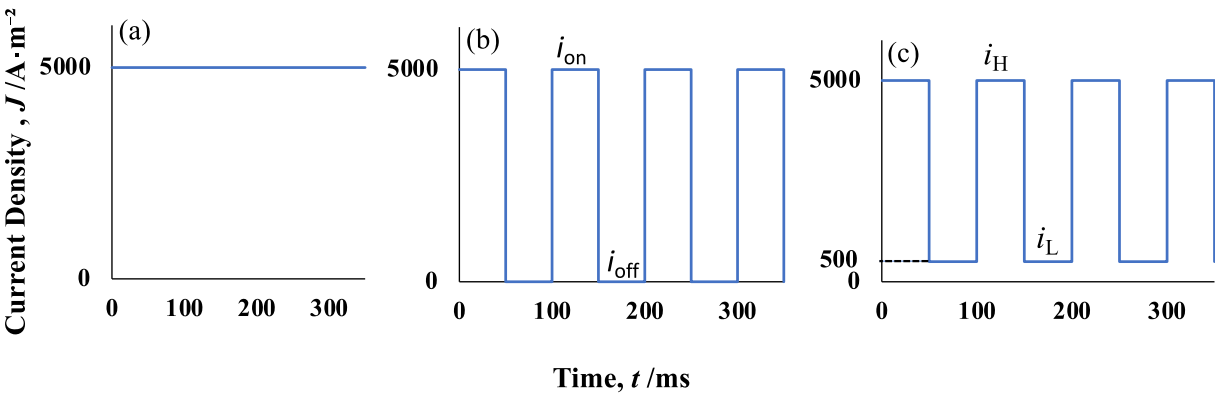

Fig. 1. Current waveforms of each type of electrolysis performed to produce films, for evaluating the microstructure and corrosion resistance. (a) Electrolysis under constant current, (b) pulse electrolysis, and (c) double-pulse electrolysis. (Online version in color.)

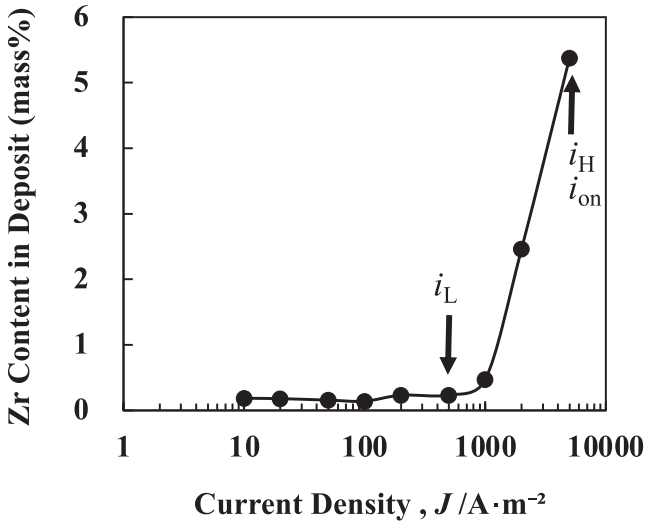

Fig. 2. Zr content in deposits obtained by electrolysis under constant current in Zn–Zr solution.

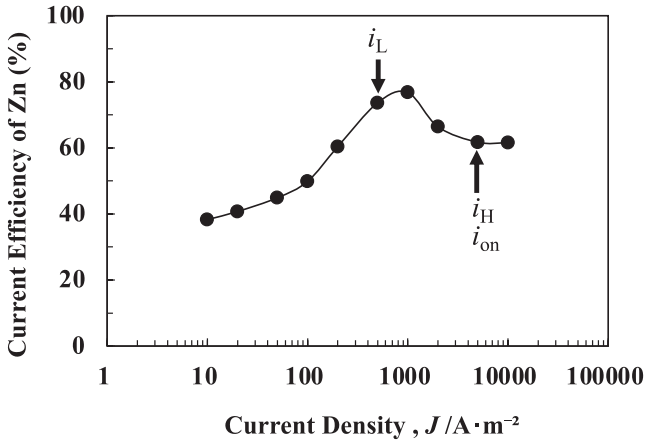

Fig. 3. Current efficiency for Zn deposition by electrolysis under constant current in Zn–Zr solution.

tion (**Fig. 4**), showing that the rate-determining process of Zn deposition was charge transfer. On the other hand, the current density of 5 000 A·m^{-2} in pulse, double-pulse, and constant-current electrolysis lay outside the Tafel's linear relationship (Fig. 4) and was close to the diffusion-limiting current density of Zn^{2+} ions, indicating that Zn deposition proceeded under the diffusion limitation of Zn^{2+} ions. The current density (i_{on}, i_H, i_L, i_{const}) for each type of electrolysis was set based on the results of the preliminary experiments under constant-current electrolysis as mentioned above (Figs. 2–4). The Zr content of the films formed in this study were calculated from the mass of Zr and Zn in the deposited films, using the following equation:

$$\text{Zr content}\left(\text{mass\%}\right) = \left[\text{mass Zr / total mass}\ \left(\text{Zn}+\text{Zr}\right)\right]\times 100$$

Each type of electrolysis was performed without stirring under the application of 10^5 C·m^{-2} of electricity and a solution temperature of 313 K. The amount of electricity of 10^5 C·m^{-2} corresponded to a film thickness of 4.7 μm, assuming the deposition of pure Zn at a current efficiency of 100%. A Cu plate (2 × 1 cm^2) was used as the cathode

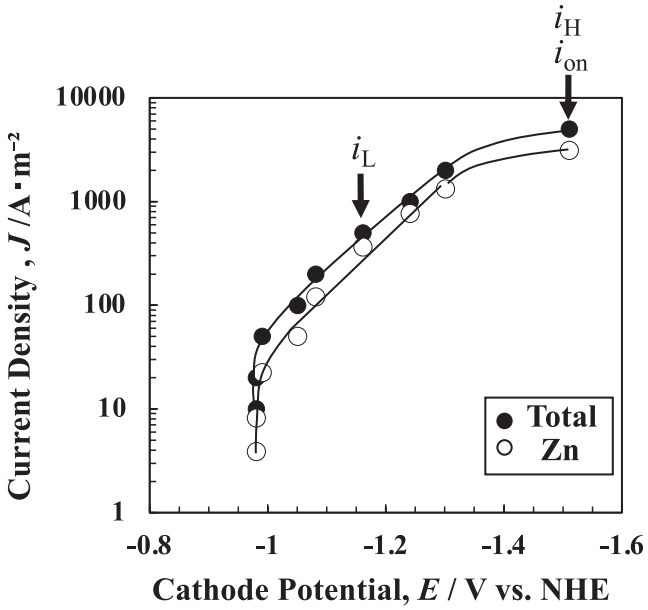

Fig. 4. Total and partial polarization curves by electrolysis under constant current in Zn–Zr solution.

and a Pt plate (2 × 1 cm^2) was used as the anode.

The deposited films were dissolved in nitric acid, and Zn and Zr were determined by inductively coupled plasma optical emission spectroscopy (ICP-OES) to obtain the compositions of the deposited films and current efficiency of Zn deposition. The partial current density for Zn deposition was calculated by multiplying the total current density by the Zn current efficiency (%)/100. When the polarization curve was measured in the preliminary experiment, electrolysis was performed at a constant current density and the potential was measured for an electricity amount of 10^5 C·m^{-2}. An Ag/AgCl electrode (saturated KCl, 0.199 V vs. normal hydrogen electrode (NHE), 298 K) was used as a reference electrode to measure the polarization curves; however, the potentials were expressed in terms of the standard hydrogen electrode.

To investigate the promotion of hydrogen evolution with the codeposition of Zr compounds with the deposited Zn, the deposited films were produced by constant-current electrolysis at 5 000 A·m^{-2} in solutions with and without ZrO^{2+} ions. Using these sample materials, the polarization curves were measured from a spontaneous potential in the cathodic-potential direction using the potential sweep method at 2.0 mV·s^{-1} in a H_2SO_4 aqueous solution of pH 2 at 313 K.

The surface morphologies and elemental distributions of the deposited films were analyzed from secondary electron images and energy-dispersive X-ray spectra (EDX) using low-acceleration-voltage scanning electron microscopy (SEM, Zeiss, ULTRA55, acceleration voltage 2–10 kV). To investigate the codeposition behavior of the Zr compound, Zn–Zr composite deposition was first performed under constant-current electrolysis of 5 000 A·m^{-2} (amount of electricity: 10^5 C·m^{-2}, film thickness: 3.0 μm, Zr content of the films: 5.3 mass%). Subsequently, Zn deposition was performed in a solution without ZrO^{2+} ions under constant-current electrolysis at 5 000 A·m^{-2} (amount of electricity: 7.5×10^4 C·m^{-2}, film thickness: 2.0 μm), and the cross sections of the double-layered films were investigated through

line analysis using EDX.

The polarization curves to evaluate the corrosion resistances of the deposited films were measured from a less noble potential than the corrosion potential (*i.e.*, in the anodic-potential direction) using the potential sweep method at 2.0 $mV \cdot s^{-1}$ in an oxygen-saturated 3% NaCl aqueous solution at 313 K.

3. Results

3.1. Effect of Electrolysis Method on the Deposition Behavior of Zn–Zr Composite

Figure 5 shows the Zr content in the deposited films obtained under each electrolysis type. The Zr content of the deposited films is the highest under constant-current electrolysis at 5 000 $A \cdot m^{-2}$, and the lowest under constant-current electrolysis at 500 $A \cdot m^{-2}$. The Zr content of the films obtained through double-pulse electrolysis (5 000/500 $A \cdot m^{-2}$) is between that obtained under constant-current electrolysis at 5 000 and 500 $A \cdot m^{-2}$. The Zr content of the films produced through double-pulse electrolysis is slightly higher than that produced through pulse electrolysis.

The hydrolysis reaction of the ZrO^{2+} ions proceeds through one of the reactions described by Eqs. (1) or (2):

$$ZrO^{2+} + 3H_2O \rightarrow Zr(OH)_4 + 2H^+ \quad \text{..... (1)}$$

$$ZrO^{2+} + H_2O \rightarrow ZrO_2 + 2H^+ \quad \text{..... (2)}$$

The faster the consumption rate of H^+ ions at the cathode layer, or the rate of hydrogen evolution, the easier the hydrolysis reaction of the ZrO^{2+} ions; therefore, the Zr content of the deposited films appears to increase with the current density. In pulse electrolysis, because the hydrogen evolution is shut off by turning off the current, the hydrolysis reaction of ZrO^{2+} ions when the current is turned on is lesser than that under constant-current electrolysis, resulting in a lower Zr content in the deposited films. In double-pulse electrolysis, as the hydrogen evolution becomes slow during low current density (500 $A \cdot m^{-2}$), the hydrolysis reaction of ZrO^{2+} ions during high current density (5 000 $A \cdot m^{-2}$) is smaller than that under constant-current electrolysis, resulting in a decrease in the Zr content in the deposited films, compared to that deposited under constant-current electrolysis.

Figure 6 shows the current efficiency for Zn deposition by each electrolysis method in Zn–Zr solution. The current efficiency for Zn deposition is the highest under constant-current electrolysis at 500 $A \cdot m^{-2}$, and decreases at 5 000 $A \cdot m^{-2}$. At 5 000 $A \cdot m^{-2}$, Zn deposition proceeds under diffusion limitation of Zn^{2+} ions, as shown in Fig. 4. The decrease in the concentration of Zn^{2+} ions in the cathode layer is expected and the current efficiency of Zn seems to decrease. In pulse electrolysis (5 000/0 $A \cdot m^{-2}$), the current efficiency of Zn is lower than that under constant-current electrolysis at 5 000 $A \cdot m^{-2}$. The deposited Zn seems to partially dissolve when the current is turned off. On the other hand, in double-pulse electrolysis (5 000/500 $A \cdot m^{-2}$), the current efficiency of Zn is between that obtained under constant-current electrolysis at 500 and 5 000 $A \cdot m^{-2}$, and close to that at 5 000 $A \cdot m^{-2}$. In the double-pulse electrolysis conducted in this study, as the electrolysis time at 500 $A \cdot m^{-2}$ is identical to that at 5 000 $A \cdot m^{-2}$, the amount of electricity at 5 000 $A \cdot m^{-2}$ is 10 times larger than that at 500 $A \cdot m^{-2}$. Therefore, the current efficiency of Zn in double-pulse electrolysis seems to be close to that under constant-current electrolysis at 5 000 $A \cdot m^{-2}$.

3.2. Effect of Electrolysis Method on the Structure of Deposited Zn–Zr Composite

3.2.1. Surface Texture

Figure 7 shows the SEM image and EDX spectra of the surfaces of the deposits obtained by constant-current electrolysis at 5 000 $A \cdot m^{-2}$ in the Zn–Zr solution. At the surface of the deposited Zn–Zr composite (Fig. 7(a)), many particles with a size of 1–5 μm and flat area are observed. In the area containing particles (① in Fig. 7(a)), Zn, Zr, and O are detected (Fig. 7(b)), indicating the codeposition of Zr hydroxide or oxide with Zn. On the other hand, in the flat area of the deposited films (② in Fig. 7(a)), Zn is mainly detected (Fig. 7(c)), showing Zn deposition. As mentioned above, under constant-current electrolysis at 5 000 $A \cdot m^{-2}$, the deposits containing Zr compounds are partially coarsened and are present nonuniformly.

Figure 8 shows the SEM image and EDX spectra of the surfaces of deposits obtained by pulse electrolysis at 5 000 and 0 $A \cdot m^{-2}$ in Zn–Zr solution. On the surface of

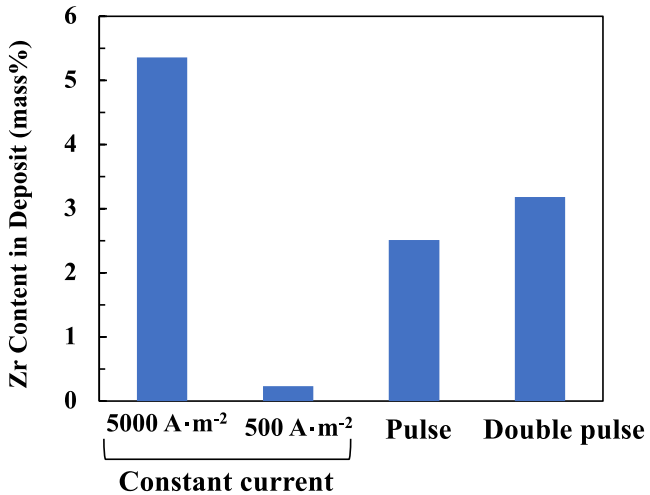

Fig. 5. Zr content in deposits obtained by each electrolysis method in Zn–Zr solution. (Online version in color.)

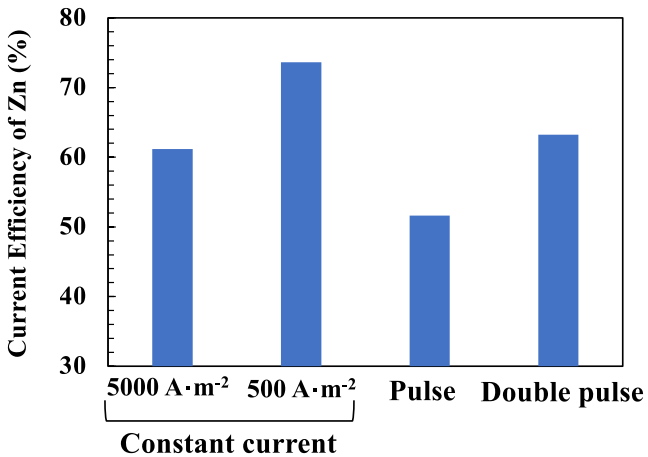

Fig. 6. Current efficiency for Zn deposition by each electrolysis method in Zn–Zr solution. (Online version in color.)

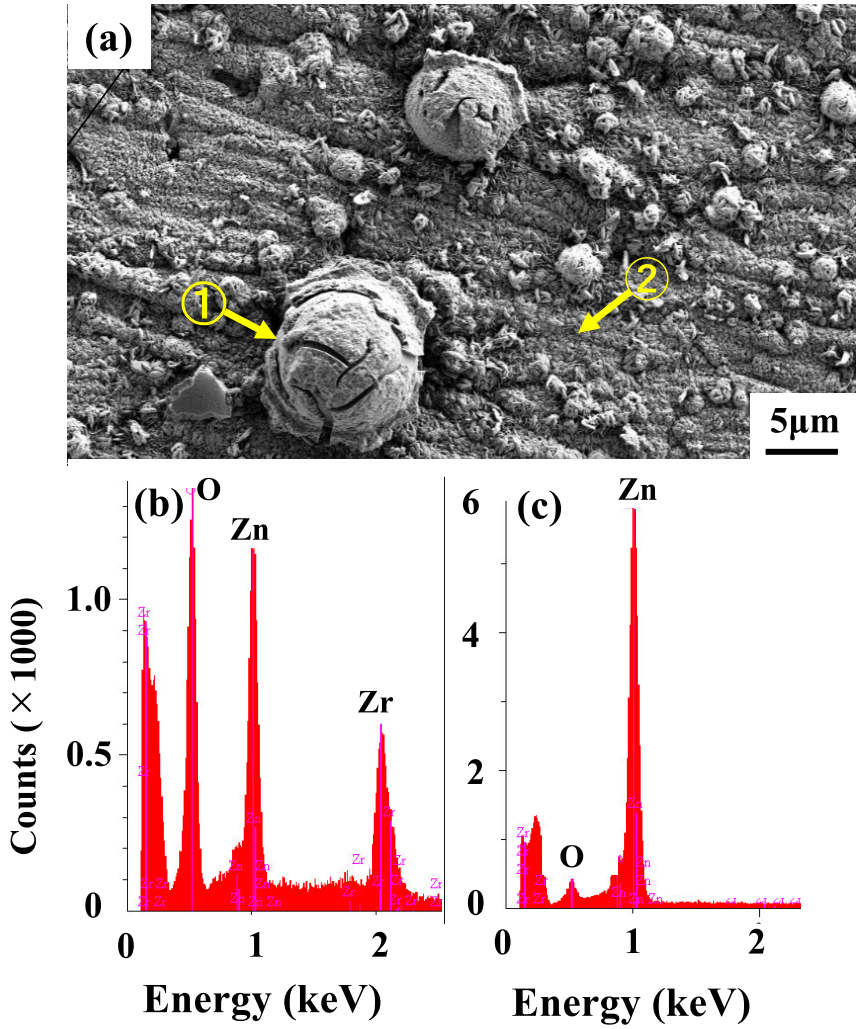

Fig. 7. SEM image and EDX spectra of surface of deposits obtained by electrolysis under constant current of 5 000 A·m^{-2} in Zn–Zr solution. [(a) SEM, (b) EDX of ①, (c) EDX of ②]. (Online version in color.)

the deposited Zn–Zr composite (Fig. 8(a)), thin-film areas containing cracks (① in Fig. 8(a)) and areas where the thin films have been exfoliated (② in Fig. 8(a)) are observed. Many cracks are present in the thin-film area and Zr and O are detected, besides Zn (Fig. 8(b)). Composite films containing Zr hydroxide or oxide seem to have been formed. Zn is mainly detected in the areas where the thin films are exfoliated (Fig. 8(c)), implying Zn deposition. In the Zn–Zr composite films obtained by pulse electrolysis, areas with composite films containing Zr compounds and those where the composite films have been exfoliated are observed (Fig. 8(a)). Therefore, the surface is observed further with lower magnification. The result is presented in **Fig. 9**. EDX analysis confirms that, in the black region of ① in Fig. 9(a), thin composite films containing Zr compounds are present on almost the entire surface (Fig. 9(b)), whereas, in the white region of ② in Fig. 9(a), Zn seems to be the only deposit (Fig. 9(c)).

Figure 10 shows the SEM image and EDX spectra of the surfaces of deposits obtained by double-pulse electrolysis at 5 000 and 500 A·m^{-2} in Zn–Zr solution. On the surface of the deposited Zn–Zr composite (Fig. 10(a)), white powdery crystals and inclined platelet crystals are observed in the SEM images. In the powdery crystals, Zn, Zr, and O are detected (Fig. 10(b)), showing Zn deposits containing Zr compounds. On the other hand, in the platelet crystals, Zn is mainly detected (Fig. 10(c)), showing the deposition of Zn with HCP structure.

3.2.2. Texture of Cross Section

Figure 11 shows the backscattered electron image and EDX mappings of a cross-section of the deposits obtained through constant-current electrolysis at 5 000 A·m^{-2} in Zn–Zr solution. Differences in composition can be observed among the areas of ①, ②, and ③ in the backscattered electron image of a cross-section of the deposited film, as shown in Fig. 11(a). The area ① corresponds to the cross-section of the particles shown in Fig. 7(a). From the particle area ①, Zn, Zr, and O are detected, showing that the particles comprise Zn and Zr compounds. In area ②, Zr and O are concentrated, indicating the presence of Zr compounds. In area ③ of the initial stage of deposition, Zn is mainly detected. As mentioned above, in the Zn–Zr composite deposition by constant-current electrolysis, the Zr compound is likely to be concentrated more in the middle and upper areas, than in the lower area, in the thickness direction of the deposited films.

Figure 12 shows the backscattered electron image (BEI) and EDX mappings of a cross-section of the deposits obtained by pulse electrolysis at 5 000 and 0 A·m^{-2} in Zn–

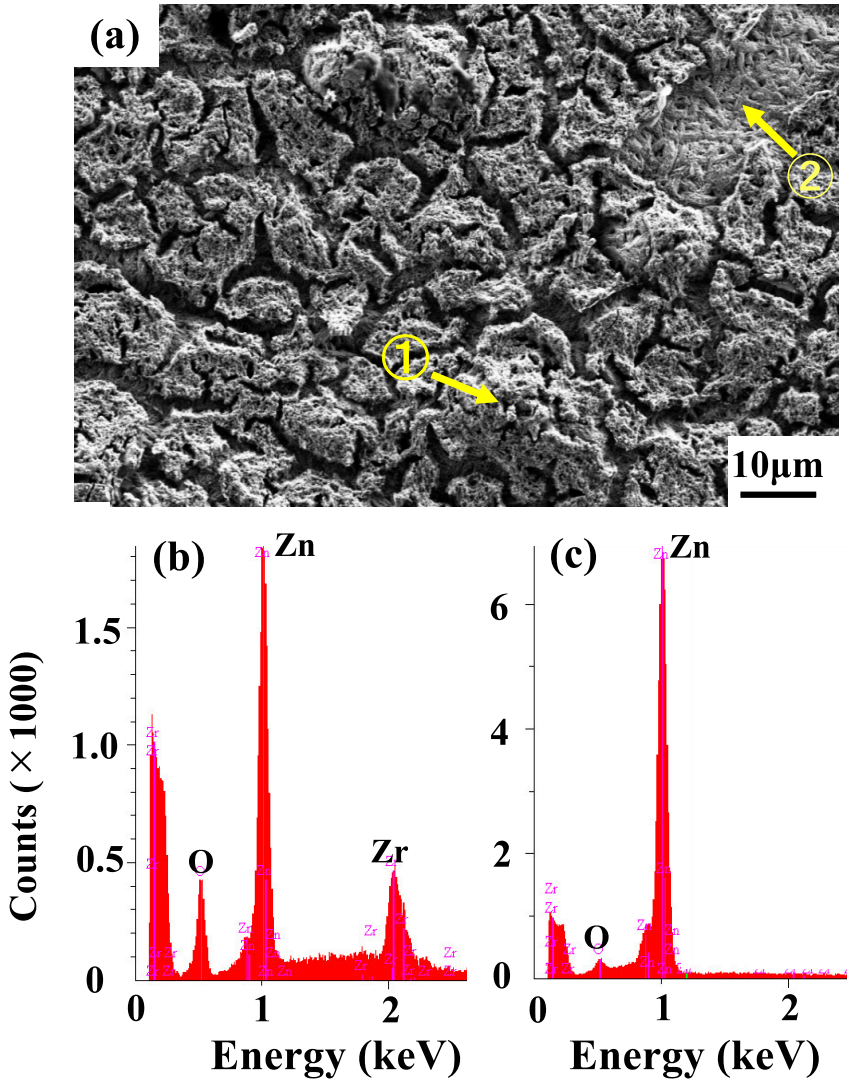

Fig. 8. SEM image and EDX spectra of surface of deposits obtained by pulse electrolysis at 5 000 and 0 A·m^{-2} in Zn–Zr solution. [(a) SEM, (b) EDX of ①, (c) EDX of ②]. (Online version in color.)

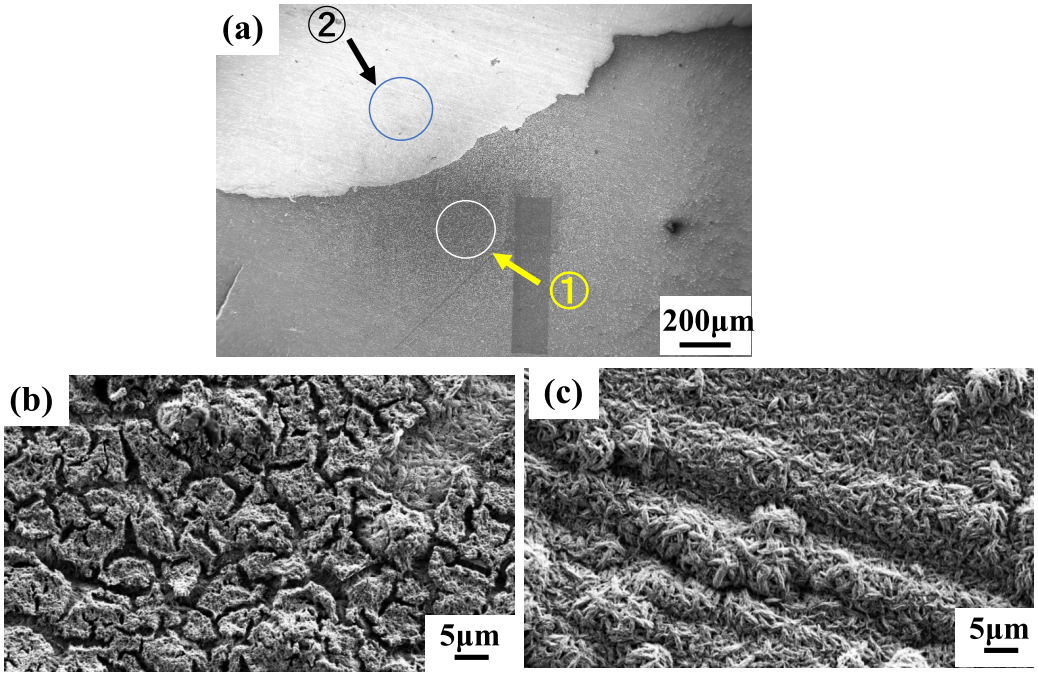

Fig. 9. SEM images of surface of deposits obtained by pulse electrolysis at 5 000 and 0 A·m^{-2} in Zn–Zr solution. [(b) Magnification of ①, (c) Magnification of ②]. (Online version in color.)

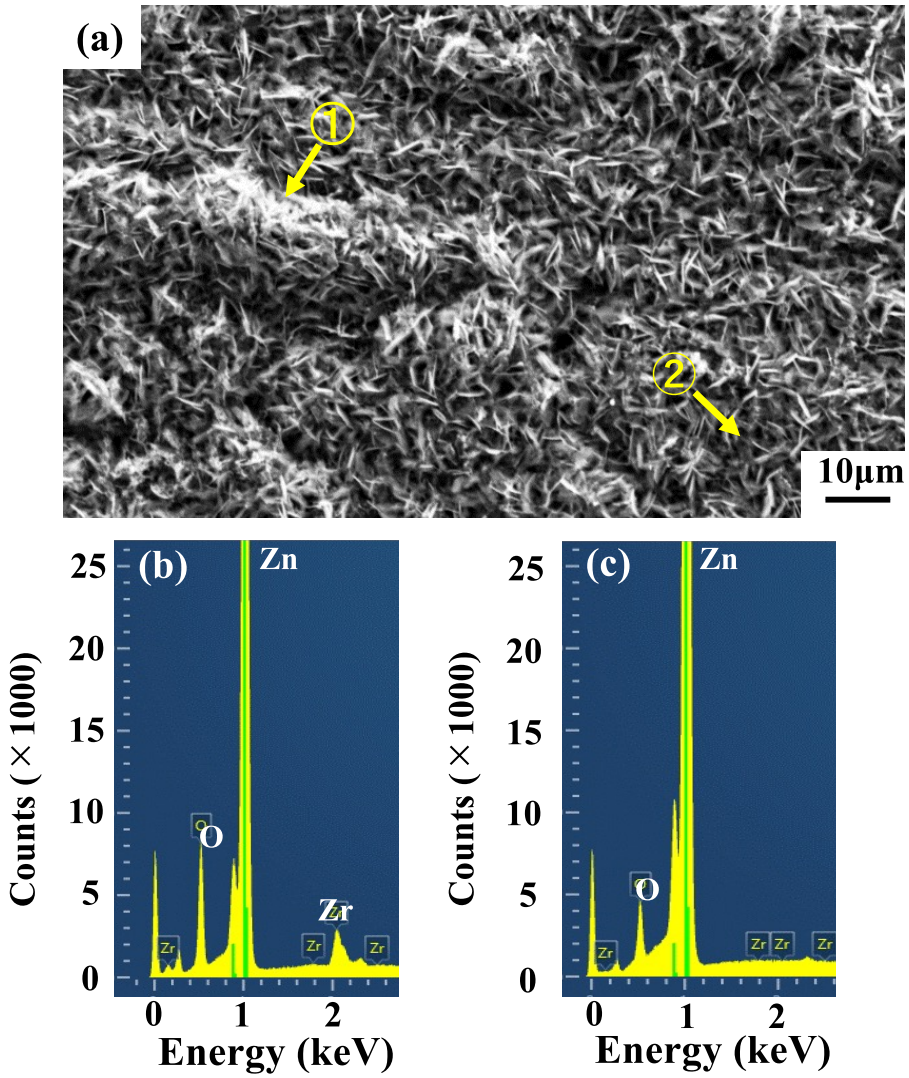

Fig. 10. SEM image and EDX spectra of surface of deposits obtained by double-pulse electrolysis at 5 000 and 500 A·m^{-2} in Zn–Zr solution. [(a) SEM, (b) EDX of ①, (c) EDX of ②]. (Online version in color.)

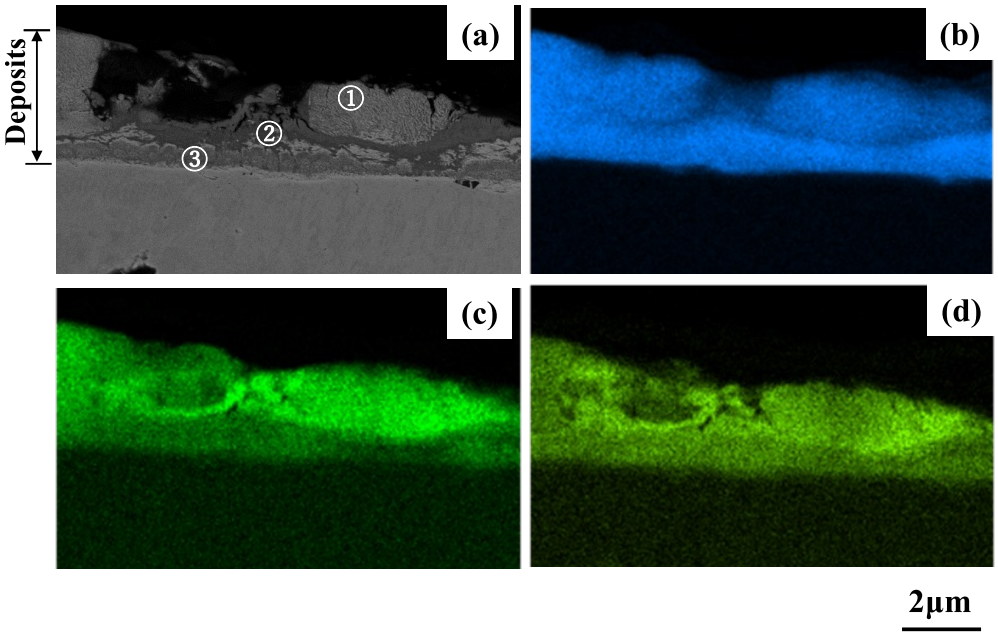

Fig. 11. (a) BEI image and (b–d) EDX mappings of a cross-section of the deposits obtained by electrolysis at constant current of 5 000 A·m^{-2} in Zn–Zr solution. [(a) BEI image, (b) Zn-K$_\alpha$ image, (c) Zr-L$_\alpha$ image, (d) O-K$_\alpha$ image]. (Online version in color.)

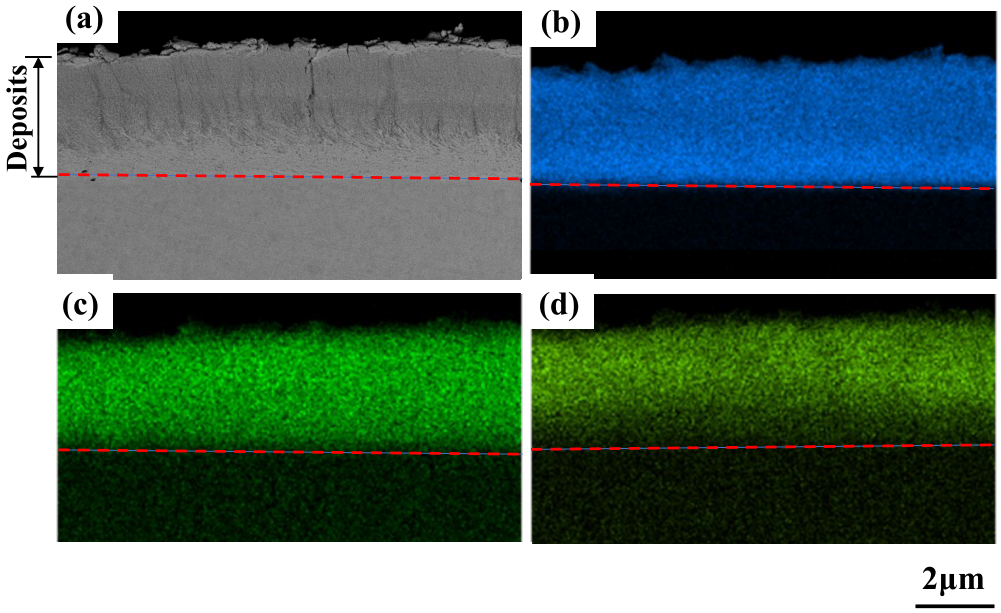

Fig. 12. (a) BEI image and (b–d) EDX mappings of a cross-section of the deposits obtained by pulse electrolysis at 5 000 and 0 A·m^{-2} in Zn–Zr solution. [(a) BEI image, (b) Zn-K$_\alpha$ image, (c) Zr-L$_\alpha$ image, (d) O-K$_\alpha$ image]. (Online version in color.)

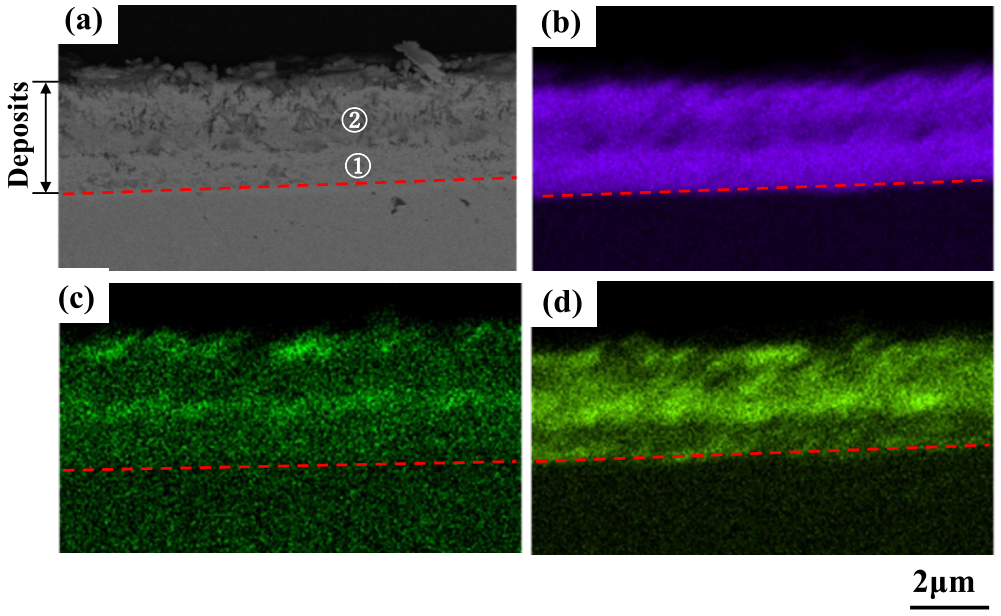

Fig. 13. (a) BEI image and (b–d) EDX mappings of a cross-section of the deposits obtained by double-pulse electrolysis at 5 000 and 500 A·m^{-2} in Zn–Zr solution. [(a) BEI image, (b) Zn-K$_\alpha$ image, (c) Zr-L$_\alpha$ image, (d) O-K$_\alpha$ image]. (Online version in color.)

Zr solution. As mentioned previously, in the deposited films obtained by pulse electrolysis, both the areas where the thin composite films containing Zr compounds are present (Fig. 9(b)) and the areas where the composite films are exfoliated (Fig. 9(c)) are observed. Figure 12 shows the cross-section of the thin composite films containing Zr compounds (Fig. 9(b)). The concentration of O is higher in the middle and upper areas, in thickness direction of the deposited films, than in the lower area. The concentration of Zn is higher in the lower area, while the concentration of Zr is slightly lower in the lower area. From the result mentioned above, it can be concluded that the Zr compounds are concentrated in the middle and upper areas in the thickness direction of the deposited films.

Figure 13 shows the BEI and EDX mappings of a cross-section of the deposits obtained by double-pulse electrolysis at 5 000 and 500 A·m^{-2} in Zn–Zr solution. In areas ① and ② of the BEI of a cross-section of the deposited films shown in Fig. 13(a), a significant difference can be observed in the morphology of the deposited films. In area ① corresponding to the first half of deposition, relatively compact crystals are observed, while coarse columnar crystals are observed in area ② corresponding to the latter half of deposition. Zr and O are largely detected at the surface and middle areas of the deposited films. That is, the Zr compound seems to be concentrated at the surface and middle areas where the

morphologies of the deposited films change.

3.3. Effect of Electrolysis Method on the Corrosion Resistance of Zn–Zr Composite Films

Figure 14 shows the polarization curves in 3 mass% NaCl solution for the deposits obtained by each electrolysis method in the Zn–Zr solution. In this study, the corrosion potential and corrosion current density are measured using the intersection point of the extrapolated straight line of the Tafel equation with the polarization curves of the anode and cathode reactions. Large differences are not observed in the corrosion potentials of the Zn–Zr composite films produced by the different electrolysis methods, but the corrosion current density is the smallest under double-pulse electrolysis, followed by that under pulse electrolysis. In the deposited films produced by double-pulse electrolysis, the reduction reaction of dissolved oxygen is the smallest. As a result, the corrosion current density becomes the smallest.

Figure 15 shows the polarization curves in 3 mass% NaCl solution for deposits obtained by double-pulse electrolysis at 5 000 and 500 $A \cdot m^{-2}$ in Zn and Zn–Zr solutions. The corrosion potential of the Zn–Zr composite films are less noble than that of the Zn films, but the corrosion current density is significantly smaller for the Zn–Zr composite films than for the Zn films. The reduction reaction of dissolved oxygen (cathode reaction in corrosion) is smaller for the Zn–Zr composite films than for the Zn films. As a result, the corrosion current density is smaller for the Zn–Zr composite films.

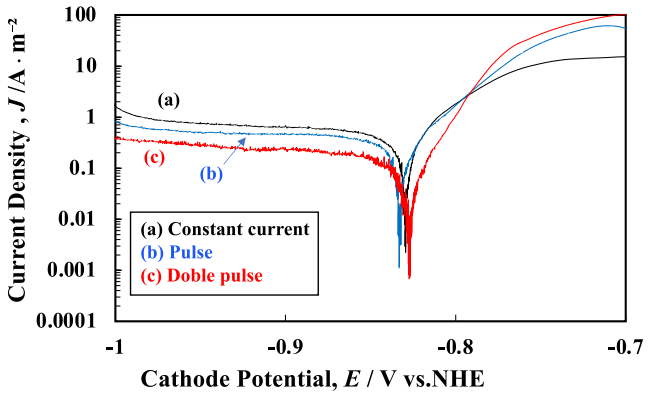

Fig. 14. Polarization curves in 3 mass% NaCl solution for deposits obtained by each electrolysis method in Zn–Zr solution. [(a) Constant current, (b) pulse, (c) double pulse]. (Online version in color.)

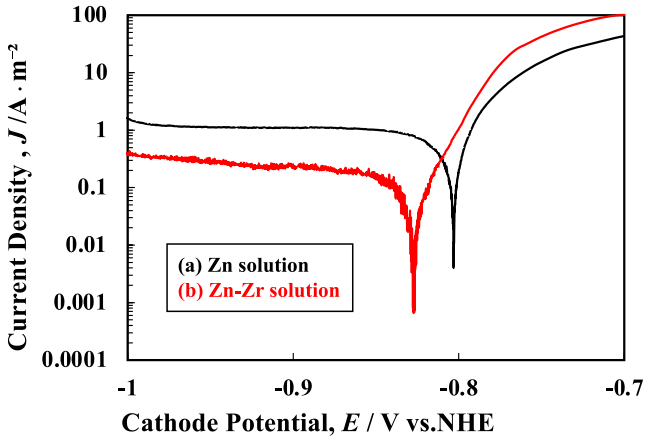

Fig. 15. Polarization curves in 3 mass% NaCl solution for deposits obtained by double-pulse electrolysis at 5 000 and 500 $A \cdot m^{-2}$ in Zn and Zn–Zr solutions. [(a) Zn, (b) Zn–Zr compound]. (Online version in color.)

4. Discussion

4.1. Effect of Electrolysis Method on the Structure of Zn–Zr Composite Films

The codeposition state of Zr hydroxide or oxide in the Zn–Zr composite films obtained by each electrolysis method is discussed below. The differences in the codeposition states of the Zr compound, among the different electrolysis methods seem to depend on the difference in the behavior of hydrogen evolution on the deposited films, which increases the pH in a focal manner. In the Zn–Zr composite films obtained through constant-current electrolysis, coarsened deposits containing Zr compounds are partially observed (Fig. 7). That is, both the hydrolysis reaction of ZrO^{2+} ions and hydrogen evolution seem to occur continuously at certain sites.

To confirm whether the Zr compound in the deposited films promotes hydrogen evolution or not, the hydrogen evolution reaction on the deposited films with and without Zr compounds is investigated in H_2SO_4 aqueous solution of pH 2. The deposited films were produced by constant-current electrolysis at 5 000 $A \cdot m^{-2}$ in solutions with and without ZrO^{2+} ions. The result is shown in **Fig. 16**. The rate of the hydrogen evolution reaction is found to be faster on films with the Zr compound than on films without the Zr compound, at all measured cathode potentials. Therefore, it is assumed that the Zr compound codeposited with Zn acts as a catalyst for hydrogen evolution, and fixes the site for both the subsequent hydrogen evolution and deposition of Zr compounds.

On the other hand, in the Zn–Zr composite films obtained by pulse electrolysis, no coarse deposits are observed, and thin films containing Zr compounds are present (Fig. 8). In pulse electrolysis, as hydrogen evolution is shut off and the

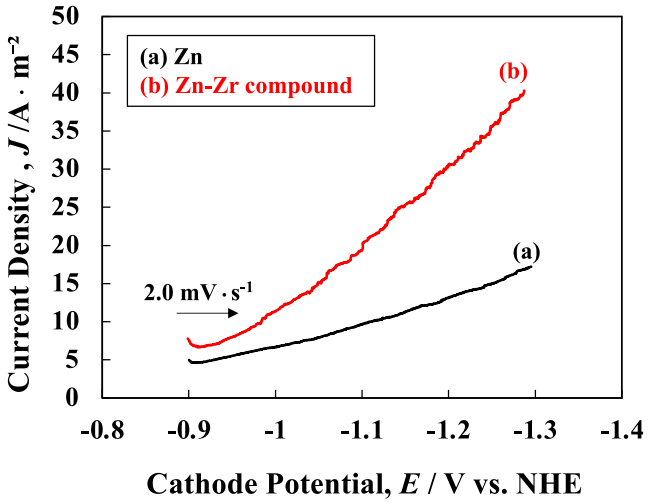

Fig. 16. Polarization curves in H_2SO_4 solution of pH 2, for deposits obtained by electrolysis under constant current of 5 000 $A \cdot m^{-2}$ in Zn and Zn–Zr solutions. [(a) Zn, (b) Zn–Zr compound]. (Online version in color.)

surface state changes owing to the slight dissolution of Zn when the current is turned off, the sites for hydrogen evolution or hydrolysis reaction of ZrO^{2+} ions are not fixed and are random. However, there are many cracks in the area of the thin films containing the Zr compounds; areas where the thin films are exfoliated are also present (Fig. 8). This is attributed to the slight dissolution of the deposited Zn when the current is turned off.

In the Zn–Zr composite films obtained by double-pulse electrolysis at high and low current densities, no coarse deposits are observed, and fine powdery crystals containing Zr compounds are deposited partially (Fig. 10). In double-pulse electrolysis, the current efficiency for Zn deposition is higher (Fig. 3) and the evolution rate and amount of hydrogen are smaller at the low current density of 500 $A \cdot m^{-2}$ than that at the high current density of 5 000 $A \cdot m^{-2}$. At a low current density, the amount of Zr compound deposited is less; the deposits are comprised almost only Zn (Fig. 5). As mentioned previously, it is thought that the Zr compounds codeposited with Zn act as catalysts for hydrogen evolution and fix the sites for the subsequent hydrogen evolution and deposition of Zr compounds. In double-pulse electrolysis, at a low current density, the hydrogen evolution reaction decreases and the surface state changes owing to the deposition of Zn alone. As a result, the sites for hydrogen evolution or hydrolysis reaction of ZrO^{2+} ions are often not fixed and are random.

Next, the codeposition state of the Zr compound in the thickness direction of the deposited films is discussed. In all three types of electrolysis— constant current, pulse and double pulse—the Zr hydroxide or oxide formed by the hydrolysis reaction of ZrO^{2+} ions is concentrated at the middle and upper areas of the films (Figs. 11–13). In the composite deposition presented in this study, Zn deposition is assumed to occur at the interface between the Zr compound layer formed at the surface by the hydrolysis reaction of ZrO^{2+} ions and the deposited film, and the Zr compound is boosted up during Zn deposition. To prove this hypothesis clearly, Zn–Zr composite deposition is first performed under constant-current electrolysis at 5 000 $A \cdot m^{-2}$ (film thickness: 3.0 μm, Zr content of the films: 5.3 mass%). Subsequently, Zn deposition is performed in the solution without ZrO^{2+} ions under constant-current electrolysis at 5 000 $A \cdot m^{-2}$ (film thickness: 2.0 μm). The EDX profile of the cross section is shown in **Fig. 17**. Even though pure Zn is deposited on the Zn–Zr composite films, the Zr compounds are concentrated at the surfaces of the deposited films, indicating that the hypothesis mentioned above is correct. That is, Zn deposition proceeds on the Zn metal (Zn deposition does not occur on the Zr compound), and the Zr compound formed by the hydrolysis reaction of ZrO^{2+} ions is boosted up in the deposited films.

On the other hand, in the Zn–Zr composite films obtained by double-pulse electrolysis, the Zr compound is codeposited in the middle areas, in addition to the surface, in the thickness direction of deposited films (Fig. 13). As mentioned previously, in double-pulse electrolysis, the deposits became relatively compact crystals in the first half of deposition, while they form coarse columnar crystals in the latter half of deposition, with the Zr compounds being concentrated at the interface. The reason for this characteristic texture is unknown, but at the interface where the crystal morphologies of the deposited films change, gaps seem to occur. The concentration of Zr compounds in the middle areas of the deposited films obtained by double-pulse electrolysis is attributed to these gaps being present. The reason for the crystal morphology of the deposited Zn changing significantly between the two halves of deposition is not clear; however, the morphology of the Zr compound possibly affects the morphology of the deposited Zn, and further investigation is required.

4.2. Effect of Electrolysis Method on the Corrosion Resistance of Zn–Zr Composite Films

As shown in Fig. 15, the reason for the corrosion potential of Zn–Zr composite films being less noble than that of the Zn films is unknown. Generally, when the cathode reaction during corrosion is suppressed or the anode reaction is promoted, the corrosion potential shifts in a less-noble direction.[32] In this study, the cathode reaction was suppressed more on the Zn–Zr composite films than on the Zn films, which seems to cause the shift of corrosion potential

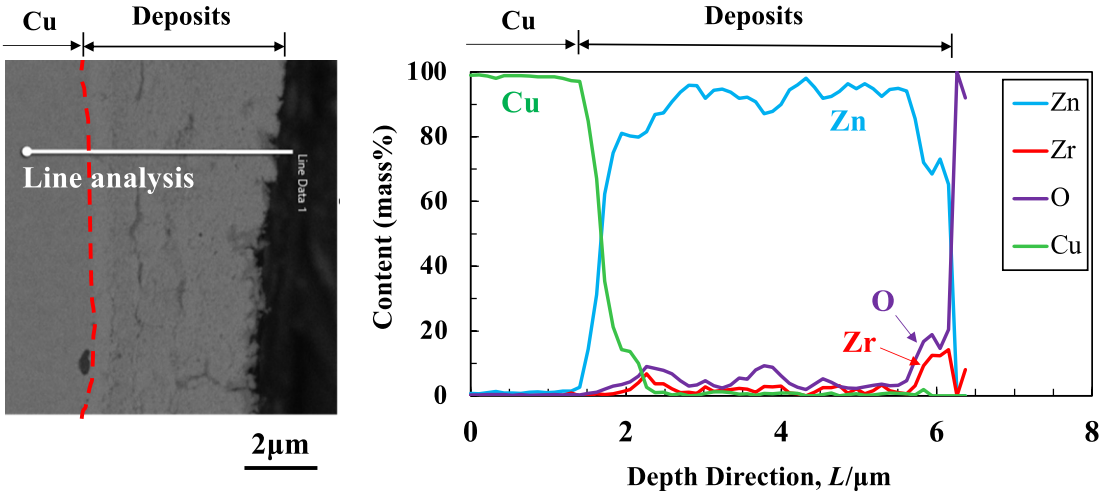

Fig. 17. Composition profile in the depth direction of deposits obtained by electrolysis under constant current of 5 000 $A \cdot m^{-2}$ in Zn and Zn–Zr solutions. (The depositions were performed first with a thickness of 3 μm in Zn–Zr solution, and then, with a thickness of 2 μm in the Zn solution). (Online version in color.)

in a less-noble direction. The reduction reaction of dissolved oxygen was the smallest on the Zn–Zr composite films obtained by double-pulse electrolysis (Fig. 14). The reduction reaction of dissolved oxygen seems to proceed on Zn metal. Therefore, the difference in the reduction current of dissolved oxygen, presented in Fig. 14, possibly depends on the difference in the area of exposure of Zn metal at the outermost surface of the deposited films, or covering with Zr compound. In constant-current electrolysis, the deposits containing Zr compounds are partially coarsened and are nonuniform, while in pulse electrolysis, thin composite films containing Zr compounds are present at certain areas and only Zn is deposited at the other areas (Fig. 8). On the contrary, in double electrolysis, fine powdery Zr compounds of size 1 μm were present on the surface (Fig. 10). Although this powdery Zr compound does not cover the entire surface uniformly, based on the Zr content of the deposited films and the morphology of the Zr compound, the net area of the Zn metal directly contacting the aqueous solution is possibly small, compared to that of other films obtained by the constant-current and pulse electrolysis methods. That is, in films obtained by double-pulse electrolysis, the area of exposed Zn metal becomes relatively small, resulting in a decrease in the reduction reaction of dissolved oxygen or the corrosion current density.

5. Conclusion

Zn–Zr compound composite films were produced by pulse and double-pulse electrolysis in nonsuspended solutions containing ZrO^{2+} ions, and their microstructures and corrosion resistance were investigated. Under constant-current electrolysis at 5 000 $A \cdot m^{-2}$, coarse granular deposits containing Zr compounds existed partially. Meanwhile, under pulse electrolysis, coarse deposits were rarely observed and both deposited films with Zr compounds and exfoliated films were observed. On the contrary, in double-pulse electrolysis at high (5 000 $A \cdot m^{-2}$) and low (500 $A \cdot m^{-2}$) current densities, coarse deposits were not observed and fine-particle deposits containing Zr compounds were observed. In pulse electrolysis, hydrogen evolution was shut off and the surface state changed with the slight dissolution of Zn when the current was turned off. In double-pulse electrolysis, the rate of hydrogen evolution decreased and the surface state changed owing to Zn deposition without the codeposition of Zr compounds, at a low current density. In these scenarios, the areas of hydrogen evolution or the areas of hydrolysis reaction of ZrO^{2+} ions were often not fixed and became random. Although the Zr compounds were concentrated in the upper areas of the deposited films, regardless of the electrolytic method, they were codeposited even in the inner parts under double-pulse electrolysis. The corrosion current density in 3 mass% NaCl solution was the smallest for the films produced by double-pulse electrolysis, followed by those produced by pulse electrolysis. In double-pulse electrolysis, the surface coverage with the Zr compound appeared to be high, and the reduction reaction of dissolved oxygen was assumed to decrease.

Acknowledgment

This work was supported by JSPS KAKENHI Grant Number JP 21H01672.

REFERENCES

1) Y. Shiohara, A. Okado, M. Abe and M. Sagiyama: *Tetsu-to-Hagané*, **77** (1991), 878 (in Japanese). https://doi.org/10.2355/tetsutohagane1955.77.7_878
2) K. Nishimura, Y. Miyoshi and T. Hada: *J. Met. Finish. Soc. Jpn.*, **38** (1987), 217 (in Japanese). https://doi.org/10.4139/sfj1950.38.217
3) I. Tari, H. Chen and H. Hayashi: *J. Surf. Finish. Soc. Jpn.*, **47** (1996), 939 (in Japanese). https://doi.org/10.4139/sfj.47.939
4) I. Tari, H. Chen and H. Hayashi: *J. Surf. Finish. Soc. Jpn.*, **47** (1996), 944 (in Japanese). https://doi.org/10.4139/sfj.47.944
5) H. Hayashi, I. Kawahara and I. Tari: *J. Surf. Finish. Soc. Jpn.*, **51** (2000), 319 (in Japanese). https://doi.org/10.4139/sfj.51.319
6) H. Nakano, S. Oue, S. Kobayashi, H. Fukushima, K. Araga, K. Okumura and H. Shige: *Tetsu-to-Hagané*, **90** (2004), 801 (in Japanese). https://doi.org/10.2355/tetsutohagane1955.90.10_801
7) S. Ishimori, M. Shimizu, S. Honda, S. Otsuka and M. Toyoda: *J. Met. Finish. Soc. Jpn.*, **28** (1977), 508 (in Japanese). https://doi.org/10.4139/sfj1950.28.508
8) H. Nakao: *J. Surf. Finish. Soc. Jpn.*, **51** (2000), 1085 (in Japanese). https://doi.org/10.4139/sfj.51.1085
9) H. Matsubara: *J. Surf. Finish. Soc. Jpn.*, **65** (2014), 88 (in Japanese). https://doi.org/10.4139/sfj.65.88
10) H. Matsubara, Y. Abe, Y. Chiba, H. Nishiyama, N. Saito, K. Hodouchi and Y. Inoue: *Electrochim. Acta*, **52** (2007), 3047. https://doi.org/10.1016/j.electacta.2006.09.043
11) Y. Umeda, Y. Sugitani, M. Miura and K. Nakai: *Tetsu-to-Hagané*, **67** (1981), 1377 (in Japanese). https://doi.org/10.2355/tetsutohagane1955.67.8_1377
12) I. Shitanda, S. Watanabe, T. Aikawa, S. Sasaki, Y. Hoshi and M. Itagaki: *J. Surf. Finish. Soc. Jpn.*, **68** (2017), 165 (in Japanese). https://doi.org/10.4139/sfj.68.165
13) Q. Hong, G. Yao and S. Chen: *Met. Finish.*, **96** (1998), 16. https://doi.org/10.1016/S0026-0576(98)80003-2
14) M. Nishira, K. Yamagishi and O. Takano: *J. Surf. Finish. Soc. Jpn.*, **44** (1993), 140 (in Japanese). https://doi.org/10.4139/sfj.44.140
15) H. Matsuda, Y. Kiyono, M. Nishira and O. Takano: *Trans. Inst. Met. Finish.*, **72** (1994), 55 (in Japanese). https://doi.org/10.1080/00202967.1994.11871023
16) S. Ankita and A. K. Singh: *Open Eng.*, **1** (2011), 234. https://doi.org/10.2478/s13531-011-0023-8
17) H. Enomoto, N. Furukawa and S. Matsumura: Fukugo Mekki (Composite Plating), Nikkan Kogyo Shimbun, Tokyo, (1989), 161 (in Japanese).
18) K. Fuchi, S. Oue, Y. Kikuchi, S. Akamatsu, Y. Kashiwa and H. Nakano: *Mater. Trans.*, **59** (2018), 1767. https://doi.org/10.2320/matertrans.M2018243
19) K. Fuchi, S. Oue, Y. Kikuchi, S. Akamatsu, Y. Kashiwa and H. Nakano: *J. Jpn. Inst. Met.*, **82** (2018), 281 (in Japanese). https://doi.org/10.2320/jinstmet.J2018020
20) H. Nakano, S. Oue, D. Kozaki, S. Kobayashi and H. Fukushima: *ISIJ Int.*, **48** (2008), 506. https://doi.org/10.2355/isijinternational.48.506
21) H. Nakano, S. Oue, Y. Annoura, T. Nagai, N. Oho and H. Fukushima: *ISIJ Int.*, **54** (2014), 1906. https://doi.org/10.2355/isijinternational.54.1906
22) S. Oue, H. Nakano, S. Kobayashi, T. Akiyama, H. Fukushima and K. Okumura: *J. Surf. Finish. Soc. Jpn.*, **53** (2002), 920 (in Japanese). https://doi.org/10.4139/sfj.53.920
23) H. Nakano, S. Oue, D. Kozaki, S. Kobayashi and H. Fukushima: *Tetsu-to-Hagané*, **93** (2007), 703 (in Japanese). https://doi.org/10.2355/tetsutohagane.93.703
24) H. Nakano, S. Oue, Y. Annoura, T. Nagai, N. Oho and H. Fukushima: *Tetsu-to-Hagané*, **100** (2014), 376 (in Japanese). https://doi.org/10.2355/tetsutohagane.100.376
25) H. Nakano, Y. Hara, S. Oue and S. Kobayashi: *Mater. Trans.*, **57** (2016), 1165. https://doi.org/10.2320/matertrans.M2016084
26) H. Nakano, Y. Hara, S. Oue and S. Kobayashi: *J. Jpn. Inst. Met.*, **80** (2016), 151 (in Japanese). https://doi.org/10.2320/jinstmet.J2015038
27) Y. Hara, D. Ueda, S. Oue and H. Nakano: *Mater. Trans.*, **60** (2019), 297. https://doi.org/10.2320/matertrans.M2018353
28) Y. Hara, D. Ueda, S. Oue and H. Nakano: *J. Jpn. Inst. Met.*, **82** (2018), 366 (in Japanese). https://doi.org/10.2320/jinstmet.J2018027
29) D. Ueda, S. Oue, T. Takasu and H. Nakano: *Mater. Trans.*, **61** (2020), 2170. https://doi.org/10.2320/matertrans.MT-M2020164
30) D. Ueda, S. Oue, T. Takasu and H. Nakano: *J. Jpn. Inst. Met.*, **84** (2020), 50 (in Japanese). https://doi.org/10.2320/jinstmet.J2019031
31) G. Ito: Fushokukagaku to Boshokugijutsu (Corrosion Science and Engineering), Corona Publishing, Tokyo, (2010), 90 (in Japanese).
32) H. H. Uhlig: Fushokuhannou to sono Seigyo (Corrosion and Corrosion Control), Sangyo Tosho, Tokyo, (1984), 48 (in Japanese).